2003

Ferroelectricity in Free Niobium Clusters

Ramiro Moro
Georgia Institute of Technology

Xiaoshan Xu
University of Nebraska-Lincoln, xiaoshan.xu@unl.edu

Shuangye Yin
Georgia Institute of Technology

Walt A. de Heer
Georgia Institute of Technology

Ferroelectricity in Free Niobium Clusters

Ramiro Moro, Xiaoshan Xu, Shuangye Yin, Walt A. de Heer

Electric deflections of gas-phase, cryogenically cooled, neutral niobium clusters [Nb_N; number of atoms (N) = 2 to 150, temperature (T) = 20 to 300 kelvin], measured in molecular beams, show that cold clusters may attain an anomalous component with very large electric dipole moments. In contrast, room-temperature measurements show normal metallic polarizabilities. Characteristic energies $k_B T_G(N)$ [Boltzmann constant k_B times a transition temperature $T_G(N)$] are identified, below which the ferroelectric-like state develops. Generally, T_G decreases [$110 > T_G(N) > 10$ K] as N increases, with pronounced even-odd alternations for $N > 38$. This new state of metallic matter may be related to bulk superconductivity.

The typical dominant response of metal clusters to an applied electric field is a polarization proportional to the magnitude of the field (*1*, *2*). This electric field E induces an electric dipole moment $P_{ind} = \alpha E$, where the polarizability $\alpha \sim R^3$ and R is the classical radius. The induced dipole causes the average internal electric field to vanish, as it does for bulk metals (*3*). In contrast, we find that Nb clusters at low temperatures frequently have a more complex response, indicating electric dipole moments that are orders of magnitude greater than P_{ind}. This ferroelectric-like property is expressed as a permanent electric dipole, P_{perm}. For low temperatures, the cluster beam was composed of two components: a normal metallic component and an anomalous ferroelectric (*4*) component. The anomalous fraction increased with decreasing temperature (T). The observed dipole moments imply internal electric fields on the order of 10^6 V/cm that are incompatible with normal metallic behavior. The large electric dipoles reflect a spontaneous-symmetry broken state (*4*, *5*, *6*), whereas their disappearance at higher temperatures indicates a dynamic mechanism that restores the symmetry (*5*–*8*). Several observed features of this extraordinary ferroelectric state in metal clusters suggest a connection with superconductivity (*3*).

Cluster dipole moments were measured by deflecting a beam of clusters in an inhomogeneous electric field (*2*, *9*–*12*). The electric response properties were determined by comparing cluster beam intensity profiles $I_N(x)$ in an applied field and in zero field (*1*, *13*, *14*). The average electric dipole moment P is found from the average deflection Δ: $P = \Delta(C\ mv^2/E)$, where m is the cluster mass, v is the velocity, and C is a constant (*1*). At room temperature, niobium cluster deflections Δ were proportional to EdE/dz (dE/dz is the field gradient perpendicular to the beam direction), consistent with normal metal cluster behavior and a (field-independent) polarizability $\alpha = P_{ind}/E$. Cold Nb clusters exhibited additional components with deflections proportional to dE/dz, indicating permanent dipole moments P_{perm}. The fraction that showed the effect and the magnitude of the dipole depended on cluster size, temperature, and electric field.

Representative beam intensity profiles, $\log_{10}[I_N(x)]$, are shown in Fig. 1 for N = 11, 12, 17, 18, and 19 atoms, at T = 300, 50, and 20 K; for E = 0 and E = 80 kV/cm. At 300 K and 80 kV/cm (Fig. 1, left column), these clusters deflect and produce rather small peak shifts on the order of 0.1 mm from their zero-field positions. The deflections are found to be strictly proportional to EdE/dz and correspond to polarizabilities $\alpha/N \sim 8$ Å^3, or induced dipole moments $P_{ind}/N = \alpha E/N \sim 10^{-3}$ debye (D) at E = 80 kV/cm.

The response changes from simple to complex when the temperature is lowered. At 50 K and 80 kV/cm (Fig. 1, middle column), N = 17 and 19 deflected proportionally to EdE/dz, but N = 11, 12, and 18 were anomalous and had tails extending from a weakly deflected central peak. The central peak deflected (essentially) proportionally to EdE/dz, but the tails deflected linearly with dE/dz, indicating permanent dipole moments (with significant intensity up to at least $P_{perm} \sim 1$ D). Some intensity at negative deflections was observed for N = 11 (and also for N = 6, 9, and 14), but not for N = 12 (nor for others); the fraction of clusters contributing to the tails increased with increasing E. This two-component behavior suggests that Nb clusters can exist in two distinct states.

At 20 K and 80 kV/cm (Fig. 1, right column), the tails extended so far that essentially all of the clusters contributing to them deflected out of the window, causing loss of the total detected intensity. The fractional lost intensity was about 0.7 for N = 11, 12, and 18. However, the loss was insignificant for N = 17 and 19. For $E > 40$ kV/cm, the central peaks of most clusters deflected proportionally to EdE/dz (notable exceptions are 9, 11, and 14, which have shoulders). Measurements for E = 10, 20, 28,

School of Physics, Georgia Institute of Technology, Atlanta GA, 30332–0430, USA.

27 January 2003; accepted 21 April 2003

40, 60, and 80 kV/cm at 20 K show that the central peak for Nb_{18}, for example, diminished uniformly with increasing electric field. Weak tails were seen at 10 kV/cm and 20 K that extended to the limits of the detector, indicating dipole moments up to 7 D. The lost intensity indicates that the dipole moment can be even greater. The surprising absence of intensity or extremely weak intensity beyond the central peak, and the decrease of the central peak with increasing field, indicate that a fraction of the clusters abruptly acquired large dipole moments as the field was increased. For example, at 20 K the loss of 28% of Nb_{14} clusters from the central peak when E was increased from 10 to 20 kV/cm indicates that the dipole moment of this fraction of the clusters increased from less than 0.1 to more than 5 D.

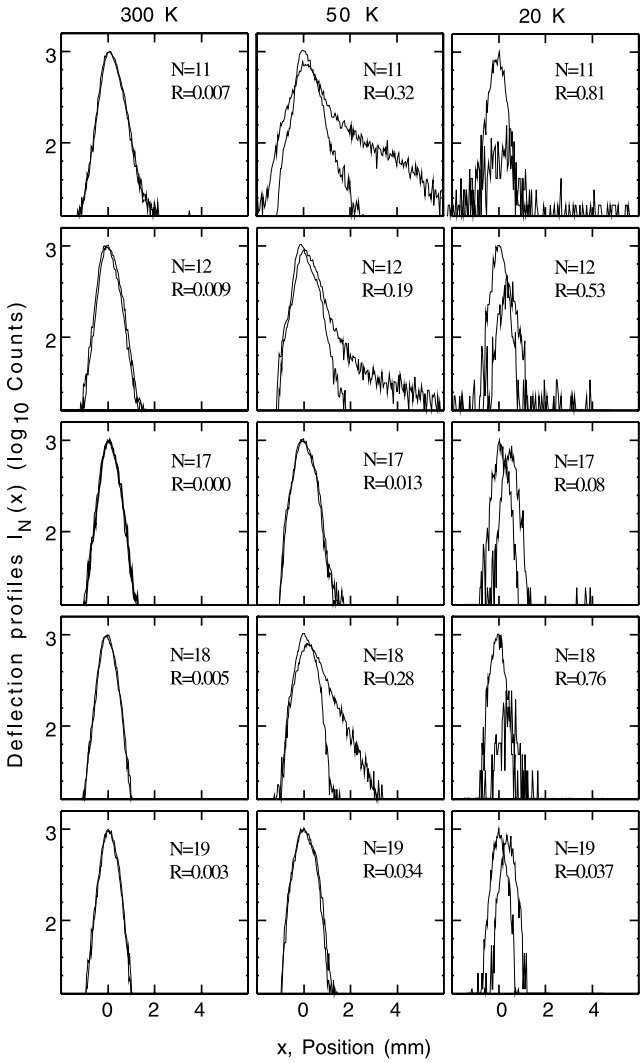

Fig. 1. Representative position-sensitive deflections of selected Nb clusters in an inhomogeneous electric field (E = 80 kV/cm) at three temperatures. The $\log_{10}$ of the measured counts versus position is shown for field off (normal trace) and field on (bold trace). At 300 K (left column), the clusters polarize and deflect weakly and proportional to EdE/dz. At 50 K (center column), several clusters exhibit extended tails that scale linearly with dE/dz, indicating a component with a large fixed electric dipole moment. All but a few clusters (that is, 2, 4, 10, 15, 16, 17, 19, 22, and 23) show this behavior. Note the intensity in the negative direction for 11 (also seen for 9 and 14). At 20 K (right column), increasing E causes a continuous reduction of the central peak (by a factor of 5 for N = 11): The majority of clusters with permanent moments are deflected beyond the limits of the detector window. R represents the fraction in the ferroelectric state.

The measured per-atom polarizabilities $\langle\alpha_N\rangle = \alpha/N = P_N/NE$ at 300 K (Fig. 2) show typical metal cluster behavior (*1*, *2*), uniformly decreasing to the bulk value (4.3 Å^3). Polarizabilities at 20 K also appear to be metallic and of the right magnitude except for the anomalous low values for 9 and 14 and the negative value for 11, caused by the negative shoulders mentioned above. However, for lower electric fields (<40 kV/cm) at 20 K, the deflections of the central peak of most clusters have both a quadratic and a linear component: $\Delta_N(E) = a_N E + b_N E^2$, where the linear component vanishes with increasing field, so that at 80 kV/cm only the quadratic component survives for most clusters. For example, for 20 kV/cm (not shown in Fig. 2), the polarizabilities $\langle\alpha_N\rangle$ of the clusters are significantly enhanced: $\langle\alpha_{13}\rangle$ = 17 Å^3 whereas $\langle\alpha_{30-100}\rangle$ range from 8 to 16 Å^3. With increasing E, the large N-dependent oscillations are reduced and the polarizabilities per atom converge to those presented in Fig. 2. At 20 K, the polarizabilities are systematically lower than those at 300 K. A similar reduction has been predicted in sodium clusters (*15*).

Figure 2 (inset) shows the dipole moments of the ferroelectric tails up to N = 32 (at 50 K). These are very large compared to the induced dipoles. For example, for N = 12, the induced dipole moment of the normal component at E =

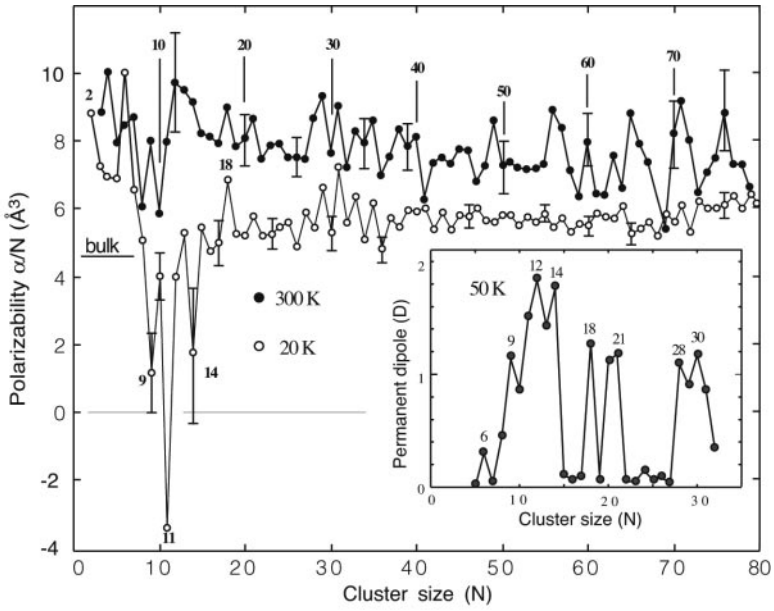

Fig. 2. Polarizabilities $\langle\alpha_N\rangle = \alpha/N$ of Nb_N. At T = 300 K, the polarizabilities show typical metallic cluster behavior with a decreasing trend, tending toward the classical value $\langle\alpha_\infty\rangle = R_N^3/N$, $(N \rightarrow \infty)$ = 4.3 Å^3. At T = 20 K, E > 40 kV/cm; and for N > 14, the polarizabilities of the central peaks are consistent with 300 K data. The observed dipole moments P_N are proportional to the applied field E, and hence the polarizability ($\alpha_N = P_N/NE$) is well defined and field-independent. This is not the case for E < 40 kV/cm, where the deflections show in addition a component with a permanent dipole moment, due to the ferroelectric fraction (Fig. 1). These permanent dipoles are so large that they are completely removed at the high fields, leaving only the normal fraction for most clusters. However, at the low fields, P_N/NE is field-dependent (it diverges at very low fields; not shown in the figure) and the polarizabilty is not defined. 9, 11, and 14 are still affected because of a residual, weak, negatively deflected shoulder of the ferroelectric fraction that is not removed even at high fields (Fig. 1; T = 20 K). (**Inset**) The measured permanent dipole moments of the tails from Fig. 1 (T = 50 K). These are orders of magnitude greater than the field-induced dipole moments.

80 kV/cm and 300 K is 0.031 D, whereas the permanent dipole moment associated with the tail extends to 1.8 D. The large disparity in these moments, and thus the large disparity in the deflections, allows the two components to be resolved even at relatively low fields.

The ferroelectric fraction can be operationally defined as the fraction that exhibits large deflections. It is measured by $R_N(T,E) = 1 - I_N(\delta x,E)/I_N(\delta x,E = 0)$, where $I_N(\delta x,E)$ is the integrated intensity within δx about the beam center [$R_N(T,E)$ is relatively insensitive to δx]. Figure 3 shows $R_N(T,E)$ for $E = 80$ kV/cm for three temperatures [$R_N(T = 300,E) < 0.003$].

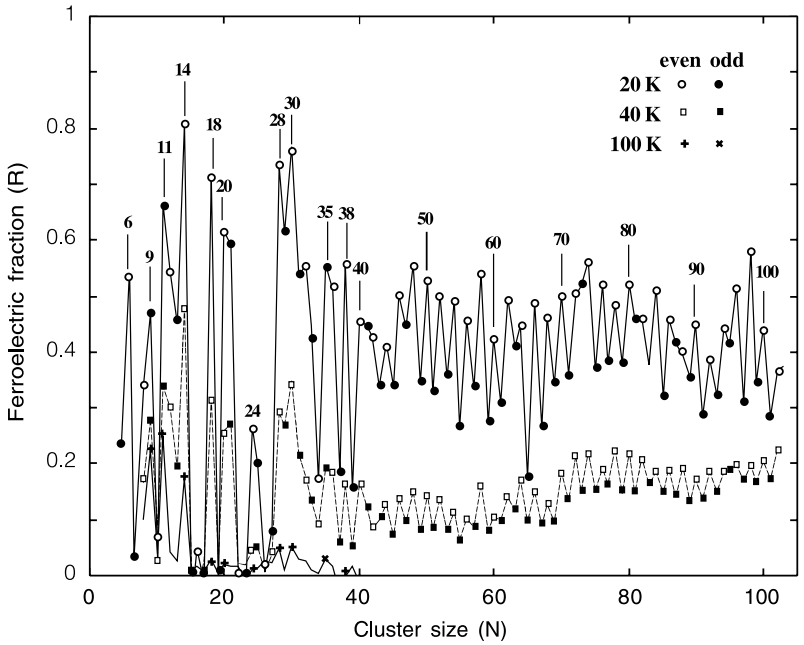

Fig. 3. The fraction R of Nb clusters in the ferroelectric state at various temperatures for 40 kV/cm. At $T = 20$ K, R presents large, reproducible, cluster size–dependent variations. In particular, 9, 11, 14, 18, 20, 21, 24, and 28 stand out, whereas 2, 10, 15, 16, 17, 19, 22, 23, and 26 are always low. The essentially uninterrupted even-odd alternation from 38 to 102 is noteworthy. At $T = 40$ K, R is reduced but the pattern is clearly discernible. At $T = 100$ K, only the major peaks ($N = 9$, 11, 14, 18, 20, and 28) stand out, whereas $R < 0.03$ for all other clusters. At T = 300 K (not shown in the figure), $R = 0 \pm 0.003$.

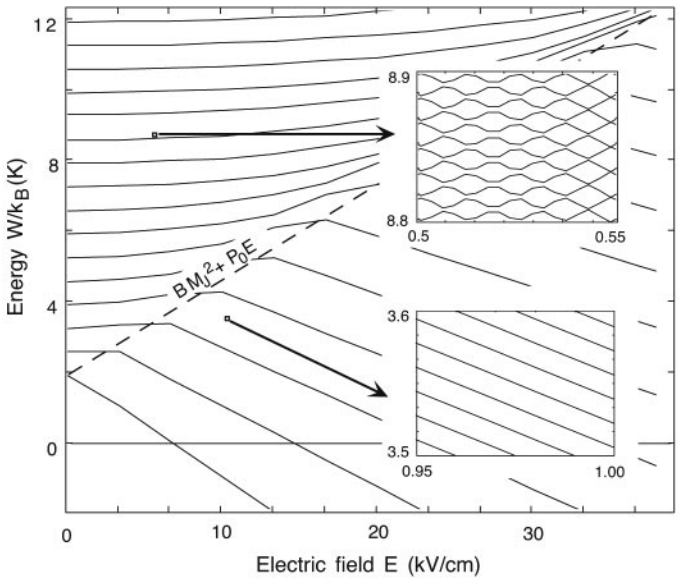

Fig. 4. Model Stark diagram for Nb_{12} for $M_J = 10$ and $P_0 = 20$ D. In an electric field, the rotational levels (taken to be equally spaced at zero field in this model; only every hundredth level is shown) split into an upgoing level and a downgoing level, according to whether the electric moment is aligned or antialigned with the angular momentum J of the cluster. All the levels anticross, producing the topology shown in the upper inset (which magnifies the indicated portion of the diagram and shows all of the levels), causing the mean slopes to be small. Beyond the crossing region, the slopes are large and negative (lower inset). The cluster dipole moments (and hence the deflections) are proportional to the slopes. Thus, a cluster on a specific energy level will abruptly present large deflections when the field is increased, so that the energy level crosses the threshold that separates the regions (dashed line $W_{thres} = BM_J^2 + P_0E$).

Large, reproducible, cluster size–dependent features are observed. For example, at $T = 20$ and 50 K, $N = 11$, 14, 18, 20, 21, 28, and 30 stand out. A remarkably intense even-odd oscillation is observed that starts at 38 and continues uninterrupted up to at least $N = 120$: $R_N(T,E)$ is enhanced for even-N clusters. In fact, from $N = 2$ to 100, the only odd-N clusters that stand out are $N = 9$, 11, and 35. The ferroelectric component is essentially absent for $N = 2$, 4, 10, 15, 16, 17, 19, 22, and 23. Furthermore, $R_N(T,E)$ rapidly diminishes with increasing temperature. At $T = 100$ K, only $N = 9$, 11, 14, 18, 20, 28, and 30 stand out.

An explanation for the development of ferroelectricity in these clusters at low temperatures is offered below. Clusters thermally equilibrate with the He gas in the source (*1*, *13*). After exiting the source, the clusters are thermally isolated and their energies W_i are fixed. Hence, the source temperature is reflected in the energy distribution of the isolated clusters and determined by Boltzmann statistics. Scaling considerations indicate that only rotations are excited in small clusters at sufficiently low temperatures (*1*). The average rotational energy level spacing is determined by the rotational constant B ($B/k_B \sim 0.1\ N^{-5/3}$ K for Nb_N), and the angular momentum J is on the order of $\sqrt{(k_BT/B)}$ (*16*). By definition, the electric dipole moment of a cluster in an electric field E is $P = dW(E)/dE$ (*17*), so that P measures this slope.

Classical models involving a permanent dipole attached to a rotor failed to reproduce the experimental deflection features (*18*, *19*). We present a quantum mechanical model (in its simplest form) to qualitatively account for the observations. The rotational energy spectrum is approximated by $W_{rot} = nB$, where n is integer and the angular momentum J is the integer part of $n^{1/2}$ (*20*). The electric dipole P_0 is assumed to be either aligned or antialigned with J. For very weak fields $W_n(n, M_J, E) = nB \pm PE$, where $P = P_0M_J/\sqrt{[J(J + 1)]}$ and $-J \le M_J \le J$ (*17*, *21*). Levels that conserve M_J are assumed to weakly interact: $<n\ M_J\ |H|\ n^*\ M_J^*> = \varepsilon(n\ n^*)\delta(M_J, M_J^*)$, where $\varepsilon(n\ n^*)$ is small but nonzero, causing crossings of levels with the same M_J to be avoided (*22*–*24*).

Figure 4 shows the resulting Stark diagram (W versus E). In the crossing region, the slopes (and consequently P) oscillate rapidly with increasing E, as shown in the top inset. This oscillatory behavior will cause the dipole moment to vanish in average in the transit through the deflecting field (for typical deflecting fields, a Nb_{10} cluster will encounter an avoided crossing for every 10 μm of deflection). For $M_J^2B + P_0E > W_n(n,M,E = 0)$, the crossings abruptly terminate, and $P = P_0M_J/\sqrt{[J(J + 1)]}$, as shown in the lower inset of Fig. 4. Thus, P abruptly changes from a small to a large value when $E = (W_n - M_J^2B)/P_0$ (*22*–*24*).

The fraction beyond the crossing region is approximately

$$R(T,E) \sim 1 - \exp(-P_0 E/kT) \quad (1)$$

Hence, R increases with increasing E and decreasing T. The dipole distribution is $F(P < P_0) = C \exp[(P - P_0)E/k_B T]$. At low temperatures, the distribution peaks at P_0 and flattens at higher temperatures, qualitatively agreeing with the observations.

However, for large E, R_N saturates to values significantly less than 1 (see the typical example in Fig. 5, inset), and this feature is not represented in the model above. Moreover, the saturation of R_N, the rate at which R_N decreases with increasing T, the reduction of the extent of the tails with increasing T, and the observation that at low temperatures the central peak itself has a normal and an anomalous component, all indicate that P_0 must be temperature-dependent. This result suggests the existence of a mode G that causes P_0 to diminish with increasing excitation energy W_G. For simplicity, we assume that G is harmonic and that P_0 is constant for $W_G < k_B T_G$ after which it vanishes. Hence

$$R_N(T,E) = \{1 - \exp[-T_G(N)/T]\} \{1 - \exp[-P_0(N)E/k_B T]\} \quad (2)$$

Figure 5 shows fitted values of T_G(N) and $P_0(N)$. For Nb_N, $T_G(N)$ decreases from 110 K for $N = 11$ to 10 K for $N = 100$, whereas $P_0(N)/N$ is of the order of 1 D. Figure 5 also shows $T_G(N)$ for vanadium (V) and for tantalum (Ta) clusters (*25*), which are systematically lower than Nb. At low temperatures, the V trimer has a clear tail extending to at least 0.27 D per atom, and the Nb trimer shows a loss of intensity (*26*). Note the similarities between structures in the T_G's in the three cases, in particular the low values for $N = 15$, 17, 22, and 23. However, an even-odd alternation is not obvious for V or Ta (likely because of poorer statistics). We note that several alloy and mixed clusters ($Nb_N V_M$, $Nb_N Co_M$, $Nb_N O_N$, and $Nb_N CO$) show similar effects; for example, $Nb_N V_M$ ($N < 20$; $M < 10$) shows the effect with properties similar to those of Nb_{N+M}.

Gas-phase measurements on Nb_N show enhanced ionization potentials for $N = 8$, 10, 16, and in the 24 to 26 region (*27*); likewise, reactivity measurements show conspicuously low reactivities for $N = 8$, 10, and 16 (*28*). Correspondingly, calculations find that $N = 4$, 8, 10, 15, and 16 are particularly strongly bound systems, suggesting the importance of the atomically closed shell bcc structure (*29*). In comparison, in our experiments, many of these clusters (in particular, 10, 15, 16, and 22 to 27) also have depressed values for T_G, which points toward a structural origin for the ferroelectric properties. In contrast, for $N > 38$, the even-odd alternations dominate the structure, which suggests that there is an overriding electronic component to the effect. There is strong evidence for shape isomers in several Nb clusters [that is, $N = 12$ (*30*)]; although we do not see clearly anomalous behavior for these clusters, it also is not obvious how the isomers might affect our measurements.

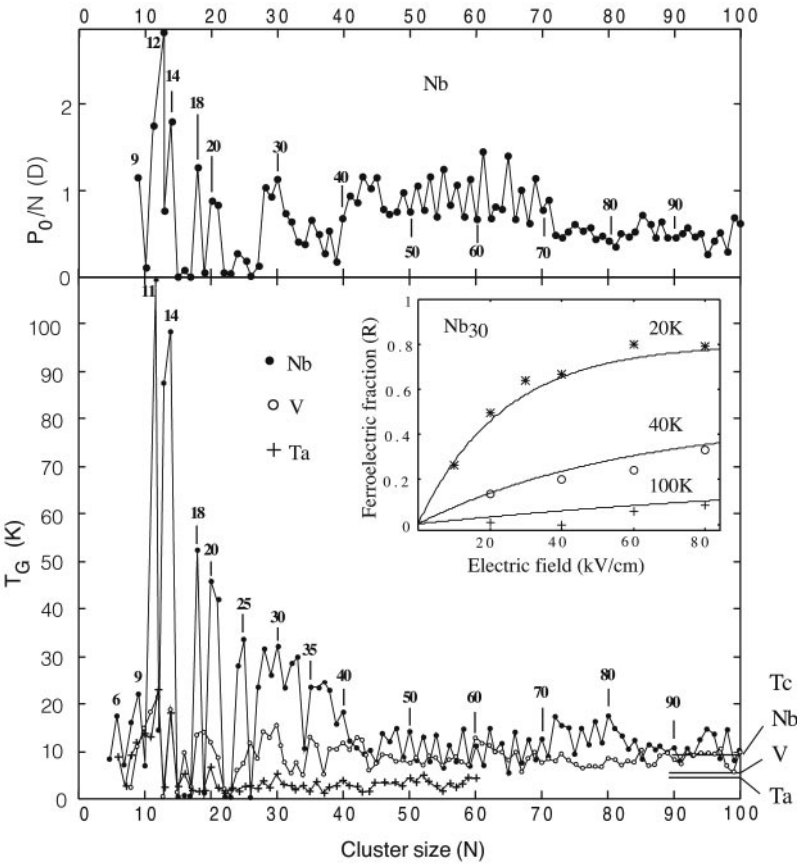

Fig. 5. Characteristic dipole moments $P_0(N)$ and energies $T_G(N)$ of ferroelectric clusters. The displayed values for Nb clusters are derived from $R_N(T,E)$ for up to six fields and at four temperatures (inset: Nb_{30} data and fit). The $T_G(N)$ values for Ta and V are derived from $R(T = 40\ K)$ data only, hence the values are not expected to be as accurate as for the Nb data. Nevertheless, the general trends are reliable. Superconducting transition temperatures (T_C) are shown on the right-hand scale.

Ferroelectricity is relatively common in bulk compound crystals, where it usually results from a spontaneous displacement of an ionic sublattice from its symmetric position, so that the unit cell acquires a dipole (*4*, *31*). However, this effect has not been observed in single-element bulk materials and certainly not in metals. In fact, a dipole density on the order of 1 D per atom generates an average internal electric field on the order of 10^6 V/cm, which clearly cannot occur in metals: Conduction electrons will neutralize these fields (*3*). The observation of the dipoles is evidence that there are essentially no free electrons. As proposed for some ferroelectrics, the spontaneous polarization could be caused by a combination of effects (such as the freezing out of metallic screening), resulting in highly polarizable ionic cores that exceed the Lorentz polarization catastrophe limit (*4*, *32*) (that is, $4\pi/3 \langle a_\infty \rangle \sim 18$ Å^3 for Nb).

In the ferroelectric state, the center of charge of the valence electrons of the clusters is displaced from that of the ions by about 1 Å to produce the observed dipoles. The shift indicates an unusual electronic charge density distribution as compared to the metallic state. The absence of free carriers and the inability of the electronic charge distribution to neutralize the dipole indicate that the structure of the conduction electrons is rigid (because it does not deform to alleviate the stress caused by the large electric fields) and collective (because all of the conduction electrons must participate) (*5*–*7*). In contrast, in the metallic state, the polarizability measurements of the same clusters indicate efficient metallic screening, so that the valence electrons are now free to respond to external fields. The reduction of the extent of the tails with increasing temperature suggests that the transition proceeds gradually. The responsible symmetry-restoring excitation is probably related to the Goldstone mode of this symmetry-broken state, as it restores the screening property of the electrons (*5*–*7*). The nature of the excitation is not clear, but it must involve the electronic charge density and it must be of very low energy.

Small net dipole moments have been predicted in metal clusters (*33*, *34*). These are related to the surface dipoles in bulk metals, which are responsible for the work function and

which vary from one crystal face to the next (*3*). The total dipole is expected to vanish with increasing size, because contributions from opposing faces tend to cancel each other. The large permanent dipoles in V, Ta, and Nb clusters and their unusual size and temperature dependence point to a different mechanism. Moreover, the fact that this extraordinary ferroelectric state is enhanced for even clusters and suppressed for odd ones is important (*35*). Electron pairing in the free electron model should result in the opposite effect: The unpaired and hence more loosely bound electron should enhance the polarizability (*1*).

Metal cluster properties are characteristically closely related to those of their bulk counterparts, allowing their evolution to be traced from the atom to the bulk (*1*). The fact that room-temperature polarizabilities of Nb clusters are well approximated using bulk metal properties even for the smallest sizes exemplifies this principle. By inference, the observed transition to a ferroelectric state at low temperatures is likely to be related to a corresponding transition in bulk Nb, and superconductivity is an obvious candidate. The assumption is strengthened by the observation that electron pairing correlations in niobium lead to superconductivity, whereas they appear to be related to the ferroelectric state in small clusters. This, combined with the correspondence of the superconducting transition temperatures of Ta, V, and Nb and the critical temperatures associated with the ferroelectric state (Fig. 5), point to a common physical origin for both properties.

References and Notes

1. W. A. de Heer, *Rev. Mod. Phys*. **65**, 611 (1993).
2. V. V. Kresin, K. D. Bonin, *Electric-Dipole Polarizabilities of Atoms, Molecules and Clusters* (World Scientific, River Edge, NJ, 1997).
3. J. M. Ziman, *Principles of Solids* (Cambridge Univ. Press, Cambridge, 1972).
4. B. Matthias, in *Ferroelectricity*, E. F. Weller, Ed. (Elsevier, Amsterdam, 1967), pp. 176–182.
5. Whenever a symmetry is spontaneously broken, according to the Goldstone theorem there will then be a gapless excitation that tends to restore the symmetry. Well-known examples are phonons for the crystalline state and spin waves for the ferromagnetic state [see, for example (*6*)].
6. P. W. Anderson, *Basic Notions of Condensed Matter Physics* (Benjamin, Menlo Park, CA, 1984).
7. P. Ring, P. Schuck, *The Nuclear Many-Body Problem* (Springer, New York, 1980).
8. H. Stern, *Phys. Rev*. **147**, 94 (1966).
9. W. D. Knight, K. Clemenger, W. A. de Heer, W. A. Saunders, *Phys. Rev. B* **31**, 2539 (1985).
10. R. Schafer, S. Schlecht, J. Woenckhaus, J. A. Becker, *Phys. Rev. Lett*. **76**, 471 (1996).
11. E. Benichou *et al*., *Phys. Rev. A* **59**, R1-R4 (1999).
12. M. B. Knickelbein, *J. Chem. Phys*. **115**, 5957 (2001).
13. G. Scoles, *Atomic and Molecular Beam Methods* (Oxford Univ. Press, Oxford, 1988); W. A. de Heer, P. Milani, *Rev. Sci. Instrum*. **62**, 670 (1991).
14. See supporting material on *Science* Online.
15. S. A. Blundell, C. Guet, R. R. Zope, *Phys. Rev. Lett*. **84**, 4826 (2000).
16. G. Herzberg, *Molecular Spectra and Molecular Structure, III Electronic Spectra and Electronic Structure of Polyatomic Molecules* (Van Nostrand, Princeton, NJ, 1966).
17. C. W. Townes, A. L. Shawlow, *Microwave Spectroscopy* (Dover, New York, 1975).
18. The classical fixed dipole on a symmetric top model by P. Dugourd *et al*. (*19*) predicts a symmetric broadening of the beam at low fields and asymmetric broadening at high fields. The model fails both qualitatively and quantitatively to describe the observed deflections, which show essentially undeflected peaks superimposed on relatively flat, extended, single-sided tails as shown in Fig. 1. The quantum mechanical model suggested here emphasizes the importance of very weak interactions between quantum mechanical levels (leading to a dense system of small avoided crossings) for which these deflection measurements are extremely sensitive: Gaps as small as 1 MHz already produce observable effects. These are in principle absent in the classical model. Also note that the observed depletions are not due to spontaneous ionization effects in the deflection fields. This possibility (as well as others) was experimentally ruled out by applying uniform electric fields of similar magnitude to the beam, which did not cause depletion.
19. P. Dugourd *et al.*, *Chem. Phys. Lett*. **336**, 511 (2001).
20. This simplified rotational spectrum is intended to demonstrate the principle that the general features are preserved when a symmetric rotor spectrum (involving J and K quantum numbers) is used (*17*).
21. In general, one expects that the dipole is coupled to a symmetry axis in the cluster [so the $P^* = P_0KM_J/J(J+1)$]; however, the model appears to fit the data better when P_0 is coupled to J. Also, it is probably more realistic to assume that for $E = 0$, the symmetry is not broken, so that P_0 should be replaced by $\sqrt{[(P_0E)^2 + G^2]}$, where G is the tunneling splitting between the aligned and antialigned states.
22. The avoided crossing model also explains anomalous magnetic deflections of paramagnetic alkali clusters (*23*, *24*).
23. W. A. de Heer, W. D. Knight, in *Proceedings of the 13th International School*, in Erice, G. Benedek, T. P. Martin, G. Pacchioni, Eds. (Springer-Verlag, Berlin, 1988), pp. 45–63.
24. W. A. de Heer, thesis, University of California, Berkeley (1985).
25. For Nb_N, similar T_G's are obtained using only $T = 20$ K and $E = 80$ kV/cm, because these fields suffice to saturate R so that $T_G = -T\log(1 - R)$. This procedure was applied to V_N and Ta_N data, because the noise levels were too high to warrant a two-parameter fit..
26. These properties already occur in trimers (but not in dimers), making them accessible for first-principles calculations.
27. R. L. Whetten, M. R. Zakin, D. M. Cox, D. J. Trevor, A. Kaldor, *J. Chem. Phys*. **85**, 1697 (1986).
28. A. Berces, P. A. Hackett, L. Lan, S. A. Mitchell, D. M. Rayner, *J. Chem. Phys*. **108**, 5476 (1998).
29. V. Kumar, Y. Kawazoe, *Phys. Rev. B* **65,** 125403 (2002).
30. M. B. Knickelbein, S. Yang, *J. Chem. Phys*., **93**, 1476 (1990).
31. R. Resta, *Rev. Mod. Phys*. **66**, 899 (1994).
32. The Lorentz polarization catastrophe results from self-polarization of a system of mutually interacting polarizable objects (polarizability α, density n) for which the susceptibilty is $\chi = n\alpha/(1 - 4\pi n\alpha/3)$. In small systems, the effect also occurs and is geometry-dependent (P. B. Allen, in preparation).
33. A. Solov'yov *et al*., *Phys. Rev. A* **65**, 053203 (2002).
34. Our low-temperature measurements on Co, Mn, Bi, and AlCo do not exhibit any evidence for permanent dipoles (W. de Heer *et al*., in preparation); alkali cluster measurements at high temperatures also have not presented evidence for permanent dipoles.
35. Magnetic deflection measurements of Nb, V, and Ta clusters at low temperatures indicate $S = 1/2$ for odd clusters and $S = 0$ for even clusters [except for Nb_2, which is a triplet (W. de Heer, in preparation)], indicating a nondegenerate energy level structure (*1*), with spacings greater than kT.

36. The authors gratefully acknowledge P. Poncharal and P. Keghelian for the development of the apparatus and R. W. Whetten and U. Landman for stimulating discussions. Financial support was provided by the U.S. Department of Defense (grant no. DAAG55-97-0133).

Supporting Online Material

www.sciencemag.org/cgi/content/full/300/5623/1265/DC1
SOM Text
Fig. S1

10 February 2003; accepted 22 April 2003